Kovove Mater. 59 2021 195–207
DOI: 10.4149/km_2021_3_195

Mechanical and corrosion characteristics of grain refined ZA-27 alloy and ZA-27/Al_2O_3 nano-composite produced by ultrasonic cavitation technique

M. T. Hayajneh*, M. A. Almomani, A. A. AL-Akailah

Industrial Engineering Department, Faculty of Engineering, Jordan University of Science and Technology, P.O. Box 3030, Irbid, 22110, Jordan

Received 11 May 2021, received in revised form 27 May 2021, accepted 10 June 2021

Abstract

In this study, the physical, mechanical, and chemical characteristics of grain refined zinc--aluminum alloy (ZA-27) and ZA-27 based nano-composite reinforced with 1wt.%Al_2O_3 nanoparticles have been investigated. Ultrasonic cavitation technique was used to fabricate these materials, and they were examined using optical microscopy, micro-Vickers hardness tester, and potentiodynamic polarization. Scanning electron microscopy (SEM) equipped with energy-dispersive X-ray spectroscopy (EDX) was used to investigate surface morphology and chemical elements of the specimens before and after corrosion testing to explain corrosion behaviors. ZA-27 alloy with fine equiaxed grains and 22 % porosity content with respect to the as-cast alloy was fabricated, resulting in a higher microhardness number. Potentiodynamic polarization test results revealed that it has better resistance for localized corrosion; the rapid dissolution of the zinc-rich phase presented in the interspacing region produces a salt layer quickly; this layer effectively protects the underlying metal surface from pits formation. The fabricated nano-composite has a porosity content of 54.2 % of the as-cast porosity content, and a smaller dendritic structure was formed with a uniform dispersion of the Al_2O_3 nanoparticles within the ZA-27 alloy matrix. Therefore, its microhardness number is greater than that of the as-cast alloy. The potentiodynamic polarization test analyses revealed that its uniform and localized corrosion resistance was improved. Micro-galvanic cells were formed between the primary and secondary phases in the small dendritic structure of the nano-composite, which improves its corrosion resistance.

K e y w o r d s: nanoparticles, aluminum dioxide, corrosion resistance, ZA-27 alloy, ultrasonic cavitation, grain refinement

1. Introduction

ZA-27 alloy is one of the most widely used zinc--aluminum alloys, as it owns high strength, high hardness, good ductility, high damping capacity, good wear, and seizure resistance [1]. The outstanding technological, economic, and co-environmental characteristics such as low casting temperature, excellent fluidity, good castability, good machining properties, low weight, low cost, and availability provide this alloy a competitive advantage over many other materials [2]. Therefore, ZA-27 becomes a candidate to replace aluminum, bronze, copper, plastic, brass, and cast iron in many applications [3]. ZA-27 alloy is usually used for bearings, bushing, plumbing fittings, thrust washers, pressure housings, builders' hardware, wear resistance parts, valves, pulleys, industrial, automotive, and farm equipment [4].

However, for high-temperature applications (above 100 ℃), a rapid deterioration of ZA-27 properties, including strength, thermal stability, and creep resistance, occurs [5]. The fabrication of extremely fine and equiaxed grains polycrystalline castings, also known as grain refinement, improves corrosion resistance, fracture toughness, and tribological properties [6]. Moreover, it facilitates the flow of molten metals during

*Corresponding author: e-mail address: hayajneh@just.edu.jo

the solidification process, eliminating shrinkage porosity and hot tearing [7]. In this method, fine spherical grain (non-dendritic) structure formed rather than columnar dendritic structure. Ultimate grain refined structures have anisotropic microstructure, isotropic properties, and less micro-segmentation into dendritic arms [6].

There are two main methods of grain refinement, chemical and physical refiners. Physical refiners have a competitive advantage over chemicals, as there is no detrimental compound formed, and the refined grain structure will be free of impurities [8]. Low--temperature pouring, rapid solidification conditions, mechanical stirring, magnetohydrodynamic stirring, spray casting, liquid casting, and ultrasonic vibrations (UST) are the main physical refining techniques [7]. UST has received strong attention as a technique for refining metallic structures. It was verified experimentally that introducing ultrasonic vibrations into molten metals eliminates the formation of columnar dendritic structures, and spherical grain structures would be attained [6].

Ultrasound is the band of sound waves with frequencies more than 20 kHz, which is greater than the audible sound frequencies range [9]. Ultrasonic waves of frequencies 20–100 kHz are used for chemical, wastewater treatment, and nanostructured material applications utilizing phenomena of cavitation (acoustic cavitation) and acoustic streaming that occurred when ultrasonic waves passed through liquids [10]. Ultrasound waves propagate in the medium longitudinally by a successive pushing action from one molecule to the next. As a result, repetitive cycles of compression (positive pressure) and rarefaction (negative pressure) between molecules will be formed [11]. When the negative pressure is lowered to less than the vapor pressure and exceeds the tensile strength of the liquid, critical molecular distance will be surpassed, and a breakdown will occur in the liquid. This rupture between molecules creates small cavities (bubbles) filled with the dissolved gases in the liquid and grow up to a specific size and then collapsed [12].

This process of micro-bubbles formation, growth, pulsation, and collapse is called acoustic cavitation, which may be stable or transient cavitation [9]. During pulsation of cavitation bubbles, dissolved gases in the liquid transfer into the bubbles due to rectified diffusion. The net diffusion of dissolved gases is an increase in the amount of transferred gases inside the cavitation bubbles, which is proportional to the intensity of the applied sound field that forces cavitation bubbles to oscillate radically and grow up to equilibrium size [13]. This is followed by collapsing these bubbles when their equilibrium size reaches resonance, i.e., a balance between the resonance frequency of the bubble and the frequency of the applied acoustic field [1].

The implosion of each cavitation bubble generates a high local temperature of about 5000 K and pressure above 1000 atm, in addition to high local heating and cooling rates above $1010\,\mathrm{K\,s^{-1}}$. Once the bubble's implosion occurs, the surrounding liquid rapidly flows to fill the void created by collapsing the bubble [14]. This liquid flow leads to producing an intense shock wave, micro-streamers, and micro-jets, which can increase turbulence inside the liquid, in addition to the generation of high-shear forces that can be useful for shearing and mixing applications [15].

Several mechanisms of how ultrasonic vibrations refine metallic structures have been proposed, all of them are based on the phenomenon that occurred when an acoustic field was applied to molten metals, such as cavitation, acoustic streams, and shock waves. These mechanisms can be divided into two groups, the first one is based on the principle of grains multiplication, and the second one is cavitation-induced heterogeneous nucleation [7]. The cooling produced in the molten metal when the probe is inserted into the molten metal is another factor that affects the grain refinement process [16].

Haghayeghi et al. [17] investigation revealed that UST is better than the chemical refiner, Al-5Ti-1B master alloy, to fabricate a grain refined AA7449 aerospace alloy with consistent mechanical properties and performance without altering its chemical composition. Qian et al. [18] study showed that the heterogeneous nucleation phenomenon resulted from the induced ultrasonic vibrations are very effective in the grain refinement of the pure magnesium and Mg-3Al--1Zn alloy.

Puga et al. [19] proved that the ultrasonic cavitation technique is more favorable than the chemical refiner, Cu-B refiner, to produce Cu-Zn alloys with enhanced mechanical properties due to the formed spherical structures instead of the original large needle block-like of the non-treated Cu-Zn alloys. Inducing the acoustic streaming into the melted soldered aluminum [20] and SAC0307 lead-free solder [21] joints efficiently refine their structures and enhance their mechanical properties. Other materials such as Mg-Sm-Al magnesium alloy [22], AA5754 aluminum alloy [23], commercially pure aluminum and Al-10Cu alloy [24], Al-2Si-2Mg-1.2Fe-(0.5,1.0)Mn alloys [25] were also treated via the ultrasonic cavitation method, and better properties were attained due to the formed fine structures.

ZA-27 alloy has been treated using several techniques of grain refinement to improve its mechanical properties. Finer structures with noticeable improvements in the strength and hardness of the ZA-27 alloy were achieved using the equal channel angular extrusion (ECAE) [26]. ZA-27 alloy with finer grains and enhanced mechanical properties was attained using different chemical refiners; these elements are titanium

and copper [27]. None of these studies investigates the effect of acoustic streaming in the microstructure and mechanical properties of ZA-27 alloy.

The metal matrix can be reinforced with ceramic or metal, and the reinforcement can be in the form of particles, fibers, whiskers, or plates. Particles are the most used type of reinforcement in metal matrix composites (MMCs) because of the attained isotropic properties of the composite. Investigations showed that reinforcement particles of size less than 100 nm could dramatically enhance properties of alloys such as strength, ductility, fatigue life, and high temperature creep resistance [28].

However, the high surface-to-volume ratio of nanoparticles increases their tendency to form clusters, making traditional manufacturing techniques improper for producing metal matrix nano-composites (MMNCs) [29]. To overcome this problem, different techniques were developed to produce MMNCs, such as vortex processing [30], high energy ball milling [31], powder metallurgy [32], stir casting [33], and ultrasonic cavitation [34]. Investigations showed that the ultrasonic cavitation technique could produce nano--composites with outstanding characteristics [35]. Alternating pressure cycles accompany introducing ultrasonic waves into the molten metal, which will cause bubble formation that grows over several cycles and then collapses violently. This collapse will cause a huge shear force that acts to break the particles and prevents their agglomeration, and helps to disperse them uniformly within different metal matrices [36].

Ultrasonic cavitation has been used for the fabrication of MMNCs. Clusters of nanoparticles can be deagglomerated by shear forces, in addition to cleaning the particle surface and reducing dissolved gases in the molten metal, which can improve wettability between nanoparticles and molten metal. At the same time, nanoparticles will be distributed and dispersed uniformly within the metal matrix due to turbulence flow inside the molten metal [9, 14].

Metals contain a significant number of inclusions that are unwettable by molten metal due to cracks and cavities on their surface. Therefore, no activities will occur during the solidification process. These cracks and cavities will be filled with molten metal by the pressure pulse generated by the cavitation process. As a result, they will act as effective heterogeneous nucleation sites, which will enhance nucleation rate during solidification. Nanoceramic particles added to molten metal for fabrication of MMNCs also act as heterogeneous nucleation sites. Hence, further refinement of grain structure will be produced [37]. Moreover, the produced ultrafine grains structure enhances the distribution of the second phase that is added to the molten metals during fabrication. Therefore, UST can be considered a good technique for the fabrication of MMNCs [38].

Choi et al. [39] used the ultrasonic cavitation technique to reinforce Al-20wt.%Si alloy with Al_2O_3 nanoparticles. The results showed that significant improvements in the yield strength, UTS, and ductility of the monolithic alloy were attained at 0.5wt.%Al_2O_3. Also, it was observed that the primary and eutectic Si particles were modified from the large star and plate shapes to smooth polygon and coralline-like shapes, respectively, which results in superior ductility enhancement.

Jia et al. [36] studied the effect of UST on the microstructure and mechanical properties of the monolithic A356 alloy and A356-Al_2O_3, SiC nanocomposites. The results revealed that UST results in monolithic material with a spherical grain structure rather than a dendritic one and produces nanocomposites of well-dispersed nanoparticle reinforcements. It was found that the use of UST to treat monolithic and nano-composites results in significant improvements in their strength and ductility.

Reinforcing ZA-27 alloy with different particles and fibers and excellent enhancements of its mechanical and tribological properties were observed [40]. Investigations showed that the corrosion resistance of ZA-27 alloy could also be improved by using different kinds of reinforcement materials [41]. MMNCs were reinforced with different nano-sized particles such as Al_2O_3, Bi_2O_3, CuO, ZrO_2, TiB_2, B_4C, SiC, and CeO_2 [42, 43]. Among these reinforcements, alumina (Al_2O_3) has significant effects on the mechanical, tribological properties, and corrosion resistance of materials [44].

In this study, ultrasonic cavitation processes will be used to fabricate a grain refined ZA-27 alloy and composites of ZA-27 alloy reinforced with Al_2O_3 nanoparticles, micro-Vickers hardness, corrosion resistance, and microstructure of the fabricated materials will be examined.

2. Materials and experimental work

2.1. Materials

ZA-27 alloy was supplied by Purity Casting Alloy Ltd. Surrey, Canada as ingots of 4 kg per ingot and with a density of 5 g cm^{-3}. The chemical composition of the ZA-27 alloy is provided in Table 1. Al_2O_3 nanoparticles (γ phase) were delivered from the Research Nanoparticles Inc. (Houston, USA) and used in as-received condition with an average size of 20 nm, 3.89 g cm^{-3} density, and 99+% purity. Moreover, 5 g of pure magnesium were added to the fabricated nano-composite to improve the wettability of Al_2O_3 nanoparticles in the molten ZA-27 alloy.

Table 1. Chemical composition of ZA-27 alloy (wt.%)

Aluminum	Cu	Mg	Fe	Cd	Zn
25.0–28.0	2.0–2.5	0.01–0.02	0.1 max.	0.005 max.	balanced

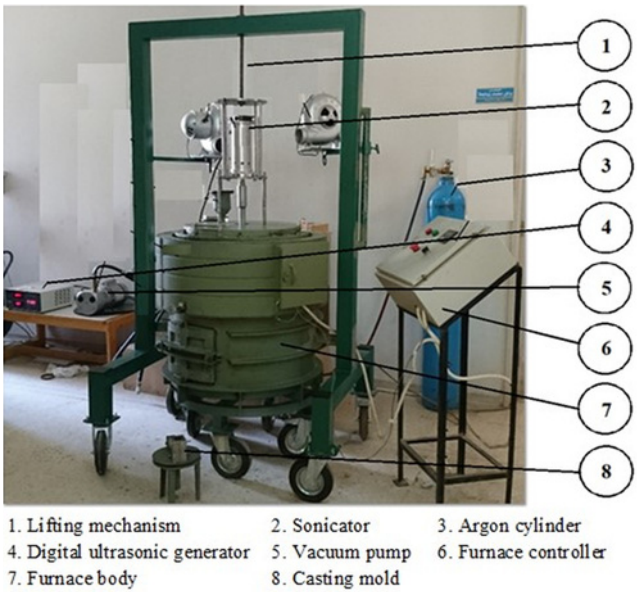

Fig. 1. The fabricated homemade electric furnace and its components.

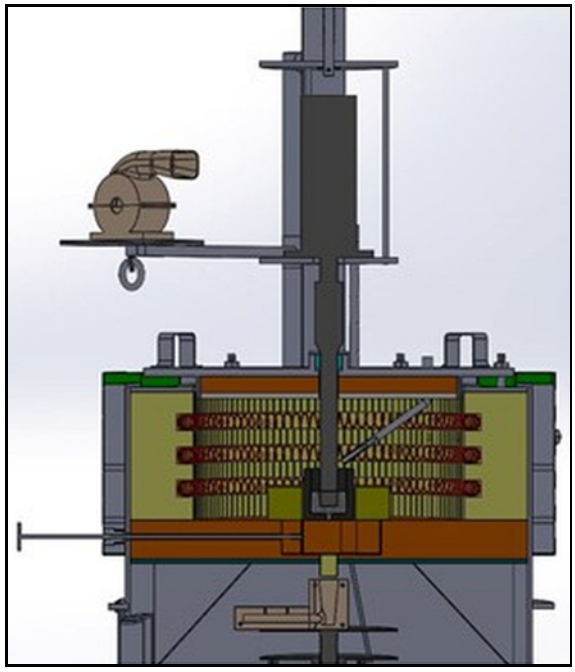

Fig. 2. A schematic diagram of the experimental setup of our homemade furnace system assisted with a sonicator.

2.2. Experimental setup

A system with controlled casting and processing conditions was designed and fabricated to produce the specimens. The processing stages were integrated into one system made of vacuum and controlled atmosphere heating resistance furnace equipped with a sonicator to disperse the nanoparticles in the metal matrix melt. Furthermore, it consists of a three-phase electric furnace assisted by many subsystems for atmospheric gases evacuation or replacement, reinforcement addition, incorporation process, and molten metal pouring. Figure 1 shows the fabricated furnace system.

2.3. Samples preparation

For each sample of the fabricated materials, an amount of the ZA-27 alloy was charged into the crucible, and the furnace was then tightly closed [45]. The pressure was reduced to –1.0 bar and then increased to –0.5 bar by introducing an inert gas (argon) into the chamber. The temperature was then increased to 550 ℃, and the material was held at this temperature for 30 minutes to ensure its solid-to-liquid transformation. For the monolithic ZA-27 alloy, the melt was then poured into the mold positioned in the lower chamber. For the ultrasonic-treated alloy, the molten ZA-27 alloy was sonicated before pouring at a power of 600 watts for 3 min.

A double layer feeding mechanism proposed by Hao [46] was used, where the ZA-27 alloy ingot was cut into small pieces, each has a small machined hole to place the reinforcement powders. These pieces are stacked at the bottom of the crucible keeping the powders covered by the stacked segments to ensure that the particles are not sucked by the vacuum. 5 g of magnesium were added to the crucible. Similar ultrasonic cavitation parameters to those used for processing ZA-27 alloy were used to produce ZA-27-1wt.%Al_2O_3 nano-composite. Figure 2 shows a schematic diagram of the experimental setup of our homemade furnace system assisted with an ultrasonic cavitation device. The amount of evaporated zinc at the processing condition is small and has no significant effect on the results. According to Shailesh [47], the magnitude of $\log(W)$ at 550 ℃ and approximately –0.5 bar (375 mm Hg) is around the –3.45 ($\mathrm{g\,cm^{-2}\,min^{-1}}$); therefore, the evaporation rate of zinc is $W = 0.000355\,\mathrm{g\,cm^{-2}\,min^{-1}}$. So, the amount of evaporated zinc was calculated to

Table 2. Density and porosity (%) of the as-cast and grain refined ZA-27 alloy and ZA-27-1wt.%Al_2O_3 nano-composite

Material	Average theoretical density ($g\,cm^{-3}$)	Average measured density ($g\,cm^{-3}$)	Average porosity (%)
As-cast ZA-27 alloy	5	4.745	5.13
Sonicated ZA-27 alloy	5	4.94	1.13
ZA-27-1wt.%Al_2O_3	4.99	4.85	2.78

be 0.3 g. In addition, aluminum forms an aluminum oxide layer on the surface of the melt, which reduces the amount of the evaporated zinc. Consequently, the amount of the evaporated zinc is actually less than 0.3 g, which has trivial effects on the density and porosity content of the fabricated materials.

2.4. Samples characterization

The density and the porosity percentile of the fabricated specimens were determined. Two cylindrical samples of identical volume from each examined composition were weighed using a four-digit sensitive balance to determine their actual density according to density law. The theoretical density of specimens was determined using the rule of mixtures, given by Eq. (1):

$$\rho_c = \rho_m \nu_m + \rho_r \nu_r, \tag{1}$$

where ρ_c is the theoretical density of the nano-composite, ρ_m is the density of the matrix, ν_m is the volume fraction of the matrix, ρ_r is the density of the reinforcement, and ν_r is the volume fraction of the reinforcement.

The average density of the fabricated monolithic ZA-27 alloy was considered as the density of the matrix. The percent porosity for each specimen was determined by comparing the actual and theoretical densities of the specimen using Eq. (2) [9]:

$$\%\text{porosity} = ((\rho_c - \rho_{EX})/\rho_c) \times 100\,\%, \tag{2}$$

where ρ_c is the theoretical density of the nano-composite and ρ_{EX} is the experimental density of the nano-composite.

A sample from each specimen was sectioned, mounted with bakelite epoxy, ground, and then polished with 0.1 μm diamond paste. Samples were then immersed for about 30 s in an etchant solution consisting of 100 ml distilled water, 5 g CrO_3, and 1 g Na_2SO_4. The general microstructure image for each specimen was obtained using an optical microscope. Vickers microhardness numbers were obtained using a micro-Vickers hardness apparatus. The samples were subjected to 200 gf load and 10 s dowel time, and then the average of nine different readings for each sample was determined.

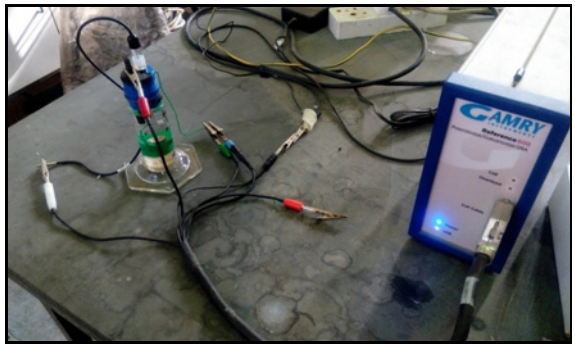

Fig. 3. Gamry Potentiostat Ref 600 connected to the customized corrosion cell.

The direct current polarization (DCP) test was used to investigate the corrosion behavior of the specimens in the 3.5wt.%NaCl electrolyte solution. Gamry potentiostat Ref 600 corrosion testing instrument was used with a graphite and saturated calomel as a counter and reference electrodes, respectively. These electrodes were held using a rubber stopper used to seal a customized glass flask to prevent the diffusion of gasses into the electrolyte. Each specimen was prepared and then connected to the device cell, as shown in Fig. 3.

SEM and EDAX were performed for two samples of monolithic ZA-27 alloy and Al_2O_3 nanoparticles to analyze their chemical composition and the average size of received nanoparticles. Also, SEM and EDAX tests were conducted for each sample before and after the corrosion test to investigate the surface morphology of the samples and to determine the dominant elements in the material and compounds on the sample surface.

3. Results and discussion

3.1. Porosity percentage

A porosity percentage of 5.13 % was measured in the fabricated as-cast ZA-27 alloy since it has a lower density than the received material, as shown in Table 2. The formation of a columnar dendritic structure with large micro-segmentation into the dendritic arms, in addition to the solidification shrinkage, re-

sulted from the used mild steel mold (high cooling rate), appreciably increases the porosity content in the fabricated as-cast ZA-27 alloy [6].

The grain refined ZA-27 alloy has a density of $4.94\,\mathrm{g\,cm^{-3}}$ and a porosity content of 1.13 %. Sonication of the molten monolithic ZA-27 alloy reduces the content of dissolved gases in the molten metal [9] and produces fine equiaxed grains that facilitate the flow of molten metal during the solidification process; hence, eliminates shrinkage porosity and hot tearing [7]. Grain refined structures of spherical shape are free of large micro-segmentations presented into dendritic arms in the columnar dendritic structures [6].

The measured density of the ZA-27-1wt.%Al_2O_3 nano-composite is $4.85\,\mathrm{g\,cm^{-3}}$, and it has a small content of porosity of 2.78 %. The solidification of molten nano-composite is controlled by the distributed nanoparticles, which produce pores in the solidified nano-composite [11]. The alternative shock waves deagglomerate the particle clusters during the sonication process and disperse them uniformly within the matrix. In addition to the added 5 grams of magnesium, the local raising in the temperature, accompanying the sonication process, cleans the surface of the particles and improves the wettability of the particles with the molten ZA-27 matrix [14]. The remaining portion of the large size clusters is formed due to the long holding time under the high temperature of the molten ZA-27 alloy.

During the solidification process, the solubility of dissolved gases in the molten metal decreases, and they are rejected with these large-size clusters in front of solidified dendrites to the inter-dendritic liquid. When the molten metal reaches its eutectic stage, pores will be formed at the inter-dendritic regions [48].

3.2. Microstructure investigation

Figure 4 shows the microstructures of the investigated materials. A dendritic structure was observed for the as-cast ZA-27 alloy, an aluminum-rich phase, primary α phase, presents as large dendrites separated by large dendritic arms spacing of the secondary eutectoid phase ($\alpha+\eta$). The small dark particles present in the interdendritic regions represent the intermetallic compound $CuZn_4$ [49].

This dendritic structure was appreciably converted to a non-dendritic structure. The two suggested mechanisms of ultra-sonication grain refinement, dendritic fragmentation, and heterogeneous nucleation, form spherical grains [7]. These grains have a patty petal-like shape of the primary α separated with thin spacing regions of the eutectoid phase ($\alpha+\eta$). Moreover, a uniform spherical structure was formed instead of course one when the AZ80 alloy was treated by the ultrasounds with a similar power value (600 W) [50].

Nanoparticles distributed within the ZA-27 matrix act as a nucleus for the crystals or restrict their growth during solidification [43]. The remaining Al_2O_3 cluster of micro-size is rejected to the inter-dendritic regions and restricts the growth of dendrites. Moreover, sonication of the molten matrix refined its structure and facilitated the flow of molten metal during solid-

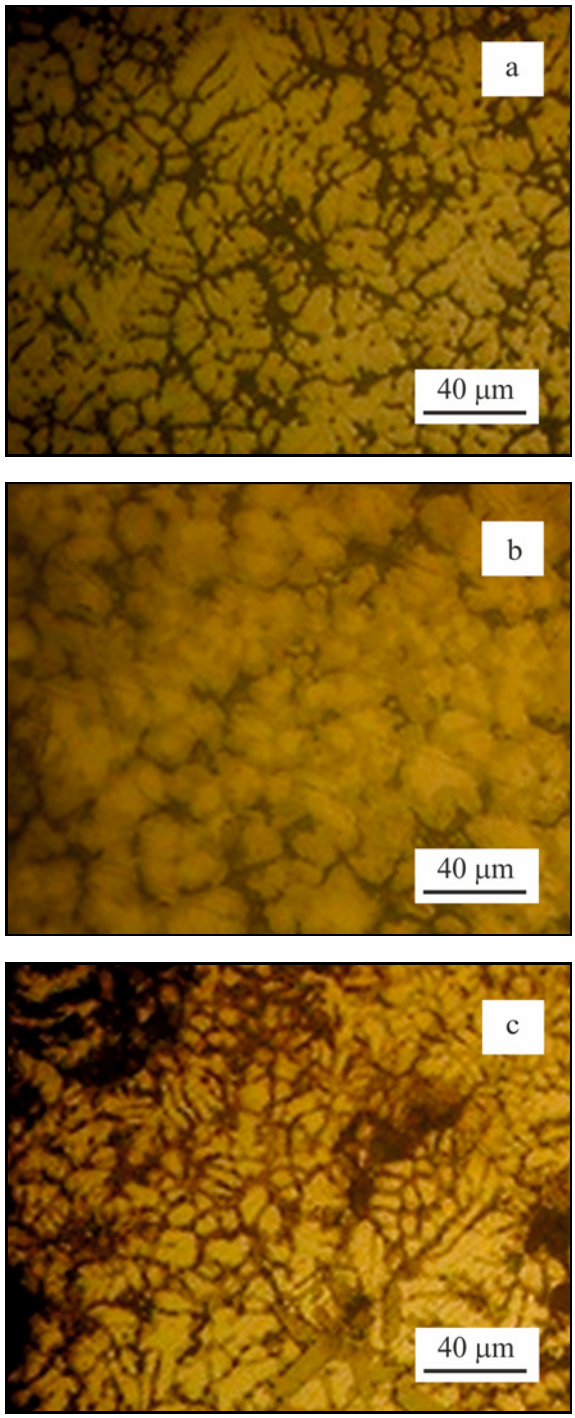

Fig. 4. General microstructures of the tested materials: (a) as-cast ZA-27 alloy, (b) grain refined ZA-27 alloy, and (c) ZA-27-1wt.%Al_2O_3 nano-composite.

Table 3. General corrosion parameters of the produced materials

Material	E_{corr} (V vs. SCE) (mV)	I_{corr} ($\mu A\ cm^{-2}$)	Corrosion rate (mpy)
As-cast ZA-27	–677.50	8.80	3.08
Sonicated ZA-27	–1000.0	4.68	4.54
Sonicated ZA-27-1wt.%Al_2O_3	–1000.09	7.64	1.91

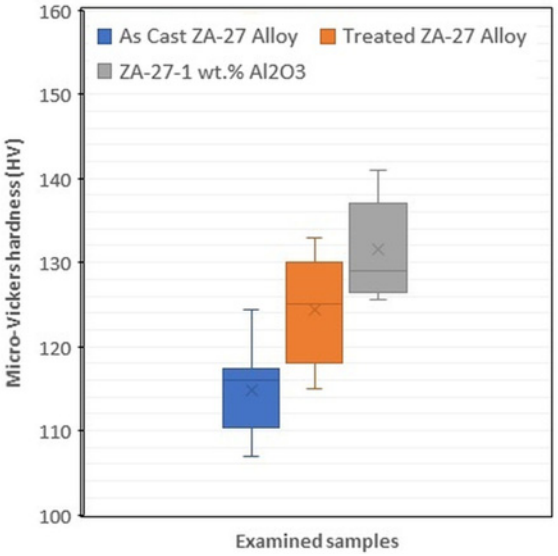

Fig. 5. Microhardness numbers of the produced as-cast and grain refined ZA-27 alloy and ZA-27-1wt.%Al_2O_3 nano--composite.

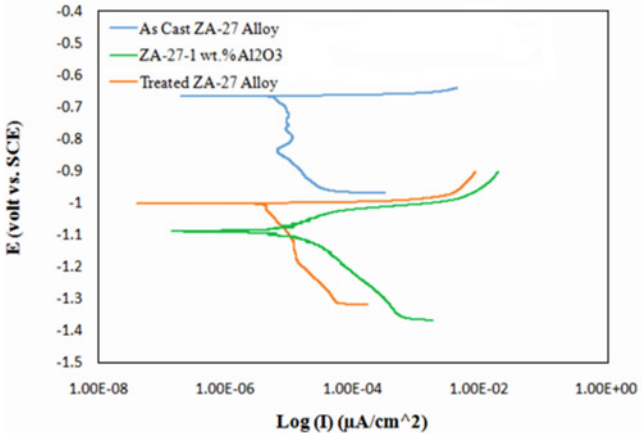

Fig. 6. The Tafel region from potentiodynamic polarization curves of the produced materials.

ification, which overall results in producing small size dendrites with light inter-dendritic spacing structures [51].

3.3. Micro-Vickers hardness

The average micro-Vickers hardness of the fabricated materials is presented in Fig. 5. The ultrasonication treatment increases the hardness of the ZA-27 alloy from 114.8 to 124.3 HV. This enhancement in the hardness is attributed to the spherical structure formed instead of the dendritic one with cracks and cavities along its dendritic arms [6]. The hardness of the ZA-27-1wt.%Al_2O_3 nano-composite is 131.6 HV. The strong shock waves and micro-streams of the cavitation deagglomerate the Al_2O_3 clusters and disperse them uniformly in a matrix with good wettability [9, 14, 15]. These particles hinder grain growth during solidification, which produces a more refined dendritic structure. Moreover, they restrict the movement of dislocations according to Orowan theory and result in harder structure [43].

3.4. Electrochemical corrosion investigation

The Tafel portions from the potentiodynamic polarization curves of the studied materials are shown in Fig. 6. The uniform corrosion parameters and the corrosion rate for each specimen were determined using the Tafel fit method, as shown in Table 3. A 3.08 mpy corrosion rate value was measured for the as-cast alloy, which is less than the maximum allowable corrosion rate in the industry and close to the value obtained by Bobic et al. [49].

The corrosion rate of the sonicated ZA-27 alloy was measured to be 4.54 mpy. Sonication of monolithic ZA-27 alloy decreases corrosion resistance of the alloy; this can be attributed to the formed structure, where the grain refined structure of the spherical primary phase (aluminum-rich phase) is less active than the interspacing phase (zinc-rich phase) that rapidly dissolves to form a protecting salt layer [52].

Reinforcing the ZA-27 alloy with Al_2O_3 nanoparticles improved its corrosion resistance and lowered its corrosion rate to be a 1.91 mpy. The presence of high electrical resistivity ($\approx 10^{15}\ \Omega\,cm$) in Al_2O_3 nanoparticles on the metal surface produces weak micro-galvanic couples between the primary and secondary phases in the small dendritic structures of reinforced ZA-27 specimens, which improves its corrosion resistance [53].

The behavior of the tested materials against the localized pitting corrosion may be measured using the parameters defined by Almomani et al. [54]. These parameters are the difference between the corrosion and re-passivation potentials ($E_{corr} - E_{RP}$) and the

Table 4. Localized corrosion parameters of the produced materials

Material	Normalized HA	$E_{corr} - E_{RP}$ (mV)
As-cast ZA-27	1.000	319.5
Sonicated ZA-27	0.392	170.0
Sonicated ZA-27-1wt.%Al_2O_3	0.557	261.0

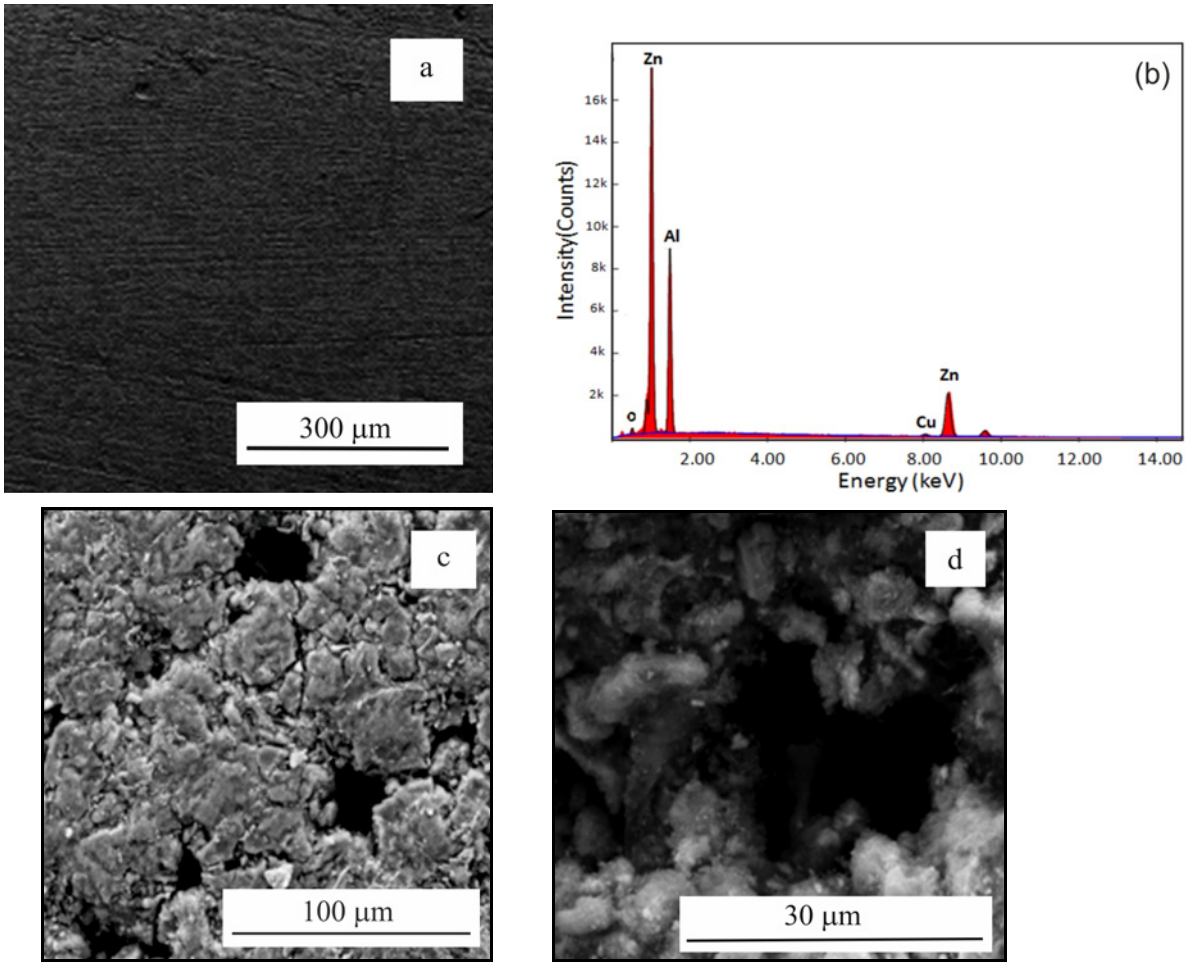

Fig. 7. (a) SEM image of the surface of as-cast monolithic ZA-27 alloy before corrosion test, (b) EDX spectrum of the surface of as-cast monolithic ZA-27 alloy before corrosion test, (c) SEM image of a cast ZA-27 monolithic alloy surface after corrosion test, and (d) SEM image showing a magnified view of one of the pits formed after potentiodynamic test of ZA-27 monolithic alloy.

bounded area between the forward and backward scans of the potentiodynamic curves, hysteresis area (H.A.). In this study, a normalized hysteresis area is determined for each specimen, in which the area of the sonicated and nano-composite specimens is determined with respect to the area of the as-cast alloy that is considered as the unity, H.A. = 1. The measured parameters for each specimen are presented in Table 4.

The as-cast ZA-27 alloy has a hypereutectoid structure consisting of a large dendritic primary α phase separated by large secondary dendritic arm spacing of the eutectoid phase ($\alpha + \eta$) [49]. These two phases have a large potential difference which forms an activated environment for galvanic corrosion. The primary phase of lower potential value acts as a cathode, while the eutectoid phase of high potential value acts as the anode. The localized corrosion occurs at the interface regions between the two phases [55].

The H.A. of the sonicated ZA-27 alloy is 0.392 of the as-cast H.A. As well, the $E_{corr} - E_{RP}$ is 170 mV for the sonicated alloy and 319.5 mV for the as-cast alloy. These values indicate that the sonication of the

ZA-27 alloy improves its resistance for pits formation. Rapid dissolution of the zinc-rich phase presented in the interspacing region produces a salt layer quickly; this layer is more effective in protecting the underlying metal surface than the layer produced on the as-cast alloy. The same results were observed by refining wrought magnesium; the refined grain structure revealed better corrosion resistance for pitting formation compared with the coarser structure [56].

It is found that the H.A. of the fabricated ZA--27-1wt.%Al_2O_3 nano-composite is 0.557 of the as-cast H.A. Furthermore, its (E_{corr} – E_{RP}) is 261 mV, which overall indicates that the nano-composite has higher resistance for localized corrosion and pits formation. The produced salt layer on the nano-composite surface protected it effectively. The salt layer that precipitated on the nano-composite surface suffered from intensive breakdowns and dissolution under higher applied potential. As the applied potential lowered, the number of breakdowns and dissolutions in the salt layer decreased and resulted in smaller H.A. and (E_{corr} – E_{RP}) values [56]. The produced grain refined structure deteriorates the resistance of the ZA-27 alloy for uniform corrosion, but on the other hand, it significantly improves its resistance for localized corrosion. Adding 1 wt.% of the Al_2O_3 nanoparticles to this alloy using the ultrasonic cavitation technique appreciably enhances its resistance for both uniform and localized corrosions.

3.5. Morphology and chemistry results

3.5.1. As-cast monolithic ZA-27 alloy

The surface of the as-cast monolithic ZA-27 alloy has scratches running parallel to the polishing lines, as shown in Fig. 7a, with few shrinkage cavities that formed during solidification or elongated tubular cavities that formed by cutting and detaching some metal during polishing. However, no pits or deep cavities are present. The EDX spectrum of the surface revealed the presence of peaks of the constituent elements of ZA-27 alloy, as shown in Fig. 7b.

Figure 7c shows the surface of a cast monolithic ZA-27 alloy after corrosion testing; the entire surface is covered with a salt film that is made of brittle materials having many cracks that may look similar to grain boundaries. These cracks may be caused by internal stresses of evolved gases from cathodic reaction or lattice mismatch between salt film and underlying metal. Also, cavities with different sizes were observed. A focused view on one of these cavities is shown in Fig. 7d, the cavity has a lacy-like appearance with a diameter of about 20 μm, but the interior surface of the cavity can't be seen due to either formation of a thick salt film of corrosion products or deepness of the cavity. The presence of deep pits is consistent with the positive hysteresis results attained in electrochemical testing (direct current polarization). The cavity is surrounded by salt particles.

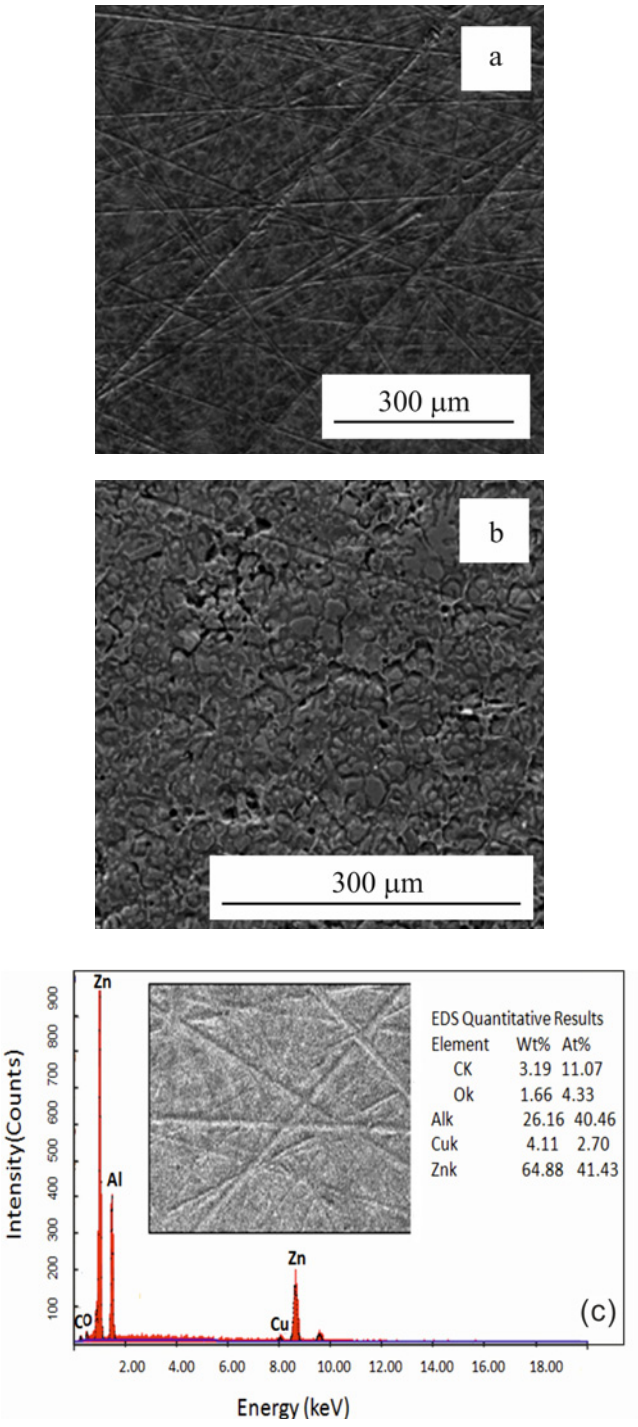

Fig. 8. SEM image of the general surface of monolithic ZA-27 alloy produced by ultrasonic cavitations: (a) before corrosion test, (b) after potentiodynamic corrosion test, and (c) EDX spectrum of the surface of ZA-27 monolithic alloy produced by ultrasonic cavitations before corrosion test.

3.5.2. Sonicated monolithic ZA-27 alloy

The SEM image in Fig. 8a shows the surface morphology of the monolithic ZA-27 alloy produced by ultrasonic cavitation. Neither pits nor shrinkage cavities were observed at the surface. Only scratch lines can be seen; these lines appear in different directions because the sample was rotated before the removal of artifacts of the previous preparation step.

The EDX spectrum of the surface before corrosion testing confirms the presence of zinc, aluminum, and copper, as shown in Fig. 8c. The quantitative analysis of the results indicates that the weight percentages of constituents' elements are very close to their values in the typical ZA-27 alloy. The polishing lines observed before the corrosion test are not seen after the corrosion testing, Fig. 8b, indicating that the surface was covered with salt film during the DCP test.

Figure 9a provides a close image of the surface after corrosion at higher magnification, shows that some cracks were filled with corrosion products; also, some pits were found randomly on the surface. However, these pits have smaller diameters than the pits observed in the as-cast monolithic alloy, as shown in Fig. 9b. Figure 9c shows the EDX spectrum with elemental quantitative results of the surface after corrosion, the reduction of the aluminum weight percentage as compared to its percentage before corrosion indicates that the most top layer has low aluminum content, which is a strong sign that most of the corrosion products are zinc-based compounds.

3.5.3. ZA-27-1wt.%Al_2O_3 nano-composite

The SEM image in Fig. 10a shows the surface of the sonicated ZA-27-1wt.%Al_2O_3 nano-composite before potentiodynamic corrosion testing, where reinforcement particles appeared as dark spots. The diameter of the reinforcement particles is less than 1 μm, as shown in the measuring dimension. The SEM image in Fig. 10b shows the surface of the sonicated ZA-27--1wt.%Al_2O_3 nano-composite after potentiodynamic corrosion testing. The surface of the nano-composite is covered with corrosion products. Shallow pits spread randomly over the surface and are surrounded by corrosion products.

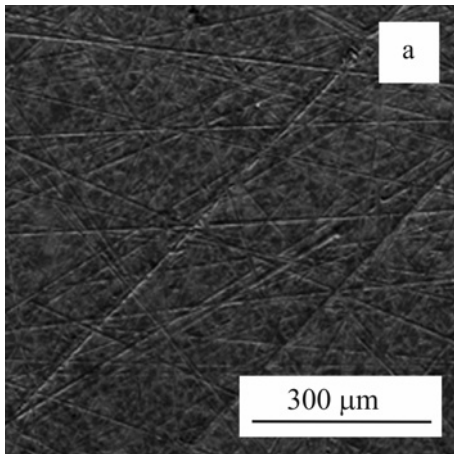

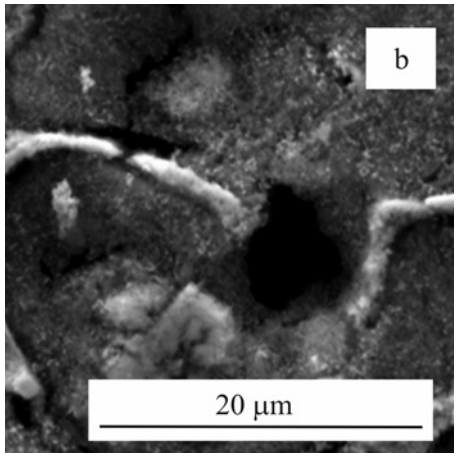

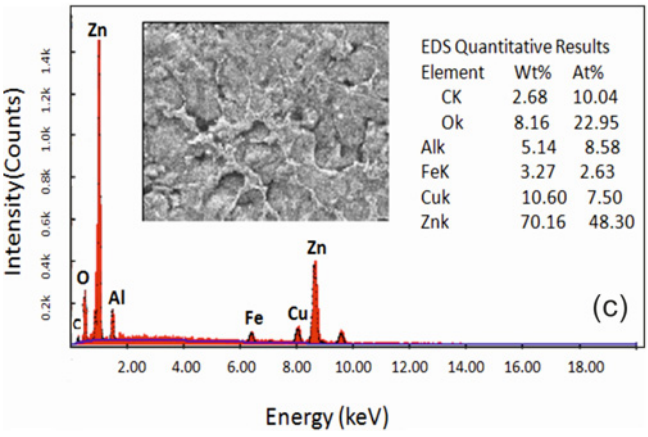

Fig. 9. (a) SEM image of the surface of ZA-27 monolithic alloy produced by ultrasonic cavitation after potentiodynamic polarization test; (b) magnified image for the area enclosed in the white rectangle of Fig. 9a, and (c) EDX spectrum and quantitative analysis of the surface of ZA-27 monolithic alloy after potentiodynamic polarization test.

4. Conclusions

1. ZA-27 alloy with fine equiaxed grains can be produced using the ultrasonic cavitation technique. Regarding the as-cast alloy, this alloy has lower porosity content, higher hardness, and better resistance for localized corrosion. However, some deterioration may occur in its resistance to uniform corrosion.

2. Ultrasonic cavitation is a good technique to fabricate nano-composites with a uniform dispersion of the particles within the metal matrix. Regarding the as-cast alloy, the produced ZA-27-1wt.%Al_2O_3 nano--composite has a finer dendritic structure with less

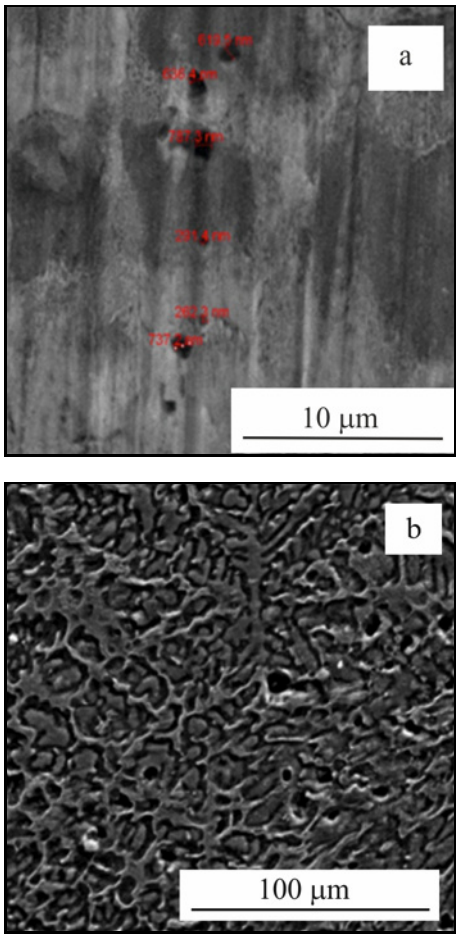

Fig. 10. (a) SEM image of the surface of sonicated ZA-27--1wt.%Al_2O_3 nano-composite before corrosion test and (b) SEM image of the surface of sonicated ZA-27-1wt.%Al_2O_3 nano-composite after potentiodynamic corrosion test.

amount of porosity, higher hardness, and enhanced resistance for uniform and localized corrosion.

3. The fabricated ZA-27-1wt.%Al_2O_3 nano-composite contains higher porosity content regarding the grain refined monolithic alloy. Nevertheless, it has higher hardness and higher resistance to uniform corrosion. Both of them have better resistance to localized corrosion.

Acknowledgements

The authors would also like to acknowledge the engineering workshop employee of JUST for their help in completing this work. This work was supported by the Deanship of Scientific Research at Jordan University of Science and Technology (JUST) with grant no. 338/2016.

References

[1] B. M. Girish, K. R. Prakash, B. M. Satish, P. K. Jain, P. Prabhakar, An investigation into the effects of graphite particles on the damping behavior of ZA-27 alloy composite material, Mater. Des. 32 (2011) 1050–1056. doi:10.1016/j.matdes.2013.10.069

[2] S. Mishra, S. Biswas, A. Satapathy, A study on processing, characterization and erosion wear behavior of silicon carbide particle filled ZA-27 metal matrix composites, Mater. Des. 55 (2014) 958–965. doi:10.1016/j.matdes.2013.10.069

[3] M. Babic, S. Mitrovic, B. Jeremic, The influence of heat treatment on the sliding wear behavior of a ZA-27 alloy, Tribol. Int. 43 (2010) 16–21. doi:10.1016/j.triboint.2009.04.016

[4] B. Girish, K. Prakash, B. Satish, P. Jain, K. Devi, Need for optimization of graphite particle reinforcement in ZA-27 alloy composites for tribological applications, Mater. Sci. Eng. A 530 (2011) 382–388. doi:10.1016/j.msea.2011.09.100

[5] G. Ranganath, S. Sharma, M. Krishna, M. Muruli, A study of mechanical properties and fractography of ZA-27/titanium-dioxide metal matrix composites, J. Mater. Eng. Perform. 11 (2002) 408–413. doi:10.1361/105994902770343935

[6] S. Jia, L. Nastac, The influence of ultrasonic stirring on the solidification microstructure and mechanical properties of A356 alloy, Chem. Mater. Eng. 1 (2013) 69–73. https:/doi.org/10.13189/cme.2013.010301

[7] T. Atamanenko, D. Eskin, L. Zhang, L. Katgerman, Criteria of grain refinement induced by ultrasonic melt treatment of aluminum alloys containing Zr and Ti, Metall. Mater. Trans. A 41 (2010) 2056–2066. doi:10.1007/s11661-010-0232-4

[8] A. Greer, Grain refinement of alloys by inoculation of melts, Phil. Trans. R. Soc. A 361 (2003) 479–495. doi:10.1098/rsta.2002.1147

[9] T. Mason, D. Peters, Practical Sonochemistry: Power Ultrasound Uses and Applications, 2nd ed., Woodhead Publishing, Cambridge, 2002.

[10] B. Sajjadi, A. Raman, S. Ibrahim, Influence of ultrasound power on acoustic streaming and micro-bubbles formations in a low frequency sono-reactor: Mathematical and 3D computational simulation, Ultrason. Sonochem. 24 (2015) 193–203. doi:10.1016/j.ultsonch.2014.11.013

[11] C. Hellier, Handbook of Nondestructive Evaluation, first ed., McGraw-Hill, New York, 2003.

[12] T. Wu, N. Guo, C. Teh, J. Hay, Advances in ultrasound technology for environmental remediation, 1st ed., Springer Science & Business Media, 2012.

[13] L. Crum, Acoustic cavitation series: part five rectified diffusion, Ultrasonics 22 (1984) 215–223. doi:10.1016/0041-624X(84)90016-7

[14] G. Cao, H. Konishi, X. Li, Mechanical properties and microstructure of SiC-reinforced Mg-(2,4)Al-1Si nanocomposites fabricated by ultrasonic cavitation based solidification processing, Mater. Sci. Eng. A 486 (2008) 357–362. doi:10.1016/j.msea.2007.09.054

[15] T. Leong, M. Ashokkumar, S. Kentish, The fundamentals of power ultrasound – A review, Acoust. Aust. 39 (2011) 54–63.

[16] J. Li, T. Momono, F. Ying, J. Zheng, Y. Tayu, Effect of ultrasonic stirring on temperature distribution and grain refinement in Al-1.65%Si alloy melt, Trans. Nonferrous Met. Soc. China 17 (2007) 691–697. doi:10.1016/S1003-6326(07)60158-7

[17] R. Haghayeghi, P. Kapranos, An investigation on physical and chemical refinement of aerospace aluminum alloys, Mater. Lett. 95 (2013) 121–124. doi:10.1016/j.matlet.2012.12.082

[18] M. Qian, A. Ramirez, A. Das, Ultrasonic refinement of magnesium by cavitation: Clarifying the role of wall crystals, J. Cryst. Growth 311(2009) 3708–3715. doi:10.1016/j.jcrysgro.2009.04.036

[19] H. Puga, J. Barbosa, J. Machado, C. Vilarinho, Ultrasonic grain refinement of die cast copper alloys, J. Mater. Process. Technol. 263 (2019) 336–342. doi:10.1016/j.jmatprotec.2018.08.034

[20] Z. Li, Z. Xu, D. Zhao, X. Liu, J. Yan, Grain refinement caused by intensified cavitation within narrow channel and its improvement to ultrasonically soldered Al joint property, Ultrason. Sonochem. 60 (2020) 104786. doi:10.1016/j.ultsonch.2019.104786

[21] H. Chen, Z. Chen, Z. Lai, Y. Li, L. Guo, The effects of ultrasonic treatments on the microstructure and mechanical properties of SAC0307 solder. J. Mater. Process. Technol. 266 (2019) 619–626. doi:10.1016/j.jmatprotec.2018.11.025

[22] X. Chen, Y. Jia, Q. Le, S. Ning, X. Li, F. Yu, The interaction between in situ grain refiner and ultrasonic treatment and its influence on the mechanical properties of Mg-Sm-Al magnesium alloy, J. Mater. Res. Technol. 9 (2020) 9262–9270. doi:10.1016/j.jmrt.2020.06.044

[23] R. Haghayeghi, E. Ezzatneshan, H. Bahai, Grain refinement of AA5754 aluminum alloy by ultrasonic cavitation: Experimental study and numerical simulation, Met. Mater. Int. 21 (2016) 109–117. doi:10.1007/s12540-014-6015-5

[24] H. Kotadia, M. Qian, D. Eskin, A. Das, On the microstructural refinement in commercial purity Al and Al-10 wt.% Cu alloy under ultrasonication during solidification, Mater. Des. 132 (2017) 266–274. doi:10.1016/j.matdes.2017.06.065

[25] H. Kotadia, M. Qian, A. Das, Microstructural modification of recycled aluminum alloys by high-intensity ultrasonication: Observations from custom Al-2Si--2Mg-1.2Fe-(0.5,1.0) Mn alloys, J. Alloys Compd. 823 (2020) 153833. doi:10.1016/j.jallcom.2020.153833

[26] R. Ahmed, A. Saleh, K. Jadee, Study the Effect of Casting Method on the Mechanical Properties of ZA-27 Alloy Formed by Equal Channel Angular Extrusion, IOP Conf. Ser.: Mater. Sci. Eng. 518 (2019) 032058. doi:10.1088/1757-899X/518/3/032058

[27] W. Krajewski, A. Greer, G. Piwowarski, P. Krajewski, Property enhancement by grain refinement of zinc--aluminum foundry alloys, IOP Conf. Ser.: Mater. Sci. Eng. 518 (2016) 012004. doi:10.1088/1757-899X/117/1/012004

[28] L. Xiaochun, Y. Yang, D. Weiss, Theoretical and experimental study on ultrasonic dispersion of nanoparticles for strengthening cast aluminum alloy A356, Metall. Sci. Technol. 26 (2008) 12–20.

[29] Y. Yang, J. Lan, X. Li, Study on bulk aluminum matrix nano-composite fabricated by ultrasonic dispersion of nano-sized SiC particles in molten aluminum alloy, Mater. Sci. Eng. A 380 (2004) 378–383. doi:10.1016/j.msea.2004.03.073

[30] S. García-Rodríguez, J. Puentes, X. Li, T. Osswald, Prediction of vortex height from mechanical mixing in metal matrix nano-composite processing by means of dimensional analysis and scaling, J. Manuf. Processes 16 (2014) 212–217. doi:10.1016/j.jmapro.2013.12.001

[31] M. Khodaei, F. Karimzadeh, M. Enayati, Fabrication of iron-alumina nano-composite powder by high energy ball milling of hematite-aluminum powder mixture, Int. J. Mod. Phys. B 22 (2008) 3233–3236. doi:10.1142/S0217979208048152

[32] S. Alam, L. Kumar, Mechanical properties of aluminium based metal matrix composites reinforced with graphite nanoplatelets, Mater. Sci. Eng. A 667 (2016) 16–32. doi:10.1016/j.msea.2016.04.054

[33] H. Ezatpour, S. Sajjadi, M. Sabzevar, Y. Huang, Investigation of microstructure and mechanical properties of Al6061-nanocomposite fabricated by stir casting, Mater. Des. 55 (2014) 921–928. doi:10.1016/j.matdes.2013.10.060

[34] M. De Cicco, X. Li, L. Turng, Semi-solid casting (SSC) of zinc alloy nano-composites, J. Mater. Process. Technol. 209 (2009) 5881–5885. doi:10.1016/j.jmatprotec.2009.07.001

[35] H. Su, W. Gao, Z. Feng, Z. Lu, Processing, microstructure and tensile properties of nano-sized Al_2O_3 particle reinforced aluminum matrix composites, Mater. Des. 36 (2012) 590–596. doi:10.1016/j.matdes.2011.11.064

[36] S. Jia, D. Zhang, Y. Xuan, L. Nastac, An experimental and modeling investigation of aluminum-based alloys and nano-composites processed by ultrasonic cavitation processing, Appl. Acoust. 103 (2016) 226–231. doi:10.1016/j.apacoust.2015.07.016

[37] S. Sardar, S. Karmakar, D. Das, Ultrasonic assisted fabrication of magnesium matrix composites: A review, Mater. Today: Proc. 4 (2017) 3280–3289. doi:10.1016/j.matpr.2017.02.214

[38] G. Totten, D. MacKenzie, Handbook of Aluminum: Vol. 1: Physical Metallurgy and Processes, 1st ed., CRC Press, Boca Raton, 2003.

[39] H. Choi, H. Konishi, X. Li, Al_2O_3 nanoparticles induced simultaneous refinement and modification of primary and eutectic Si particles in hypereutectic Al-20Si alloy, Mater. Sci. Eng. A 541 (2012) 1591–1565. doi:10.1016/j.msea.2012.01.131

[40] S. Yu, Z. He, K. Chen, Dry sliding friction and wear behaviour of short fibre reinforced zinc-based alloy composites, Wear 198 (1996) 108–114. doi:10.1016/0043-1648(96)06940-2

[41] S. Sharma, D. Somashekar, B. Satish, A note on the corrosion characterisation of ZA-27/zircon particulate composites in acidic medium, J. Mater. Process. Technol. 118 (2001) 62–64. doi:10.1016/S0924-0136(01)00864-0

[42] P. Magesan, P. Ganesan, M. Umapathy, Ultrasonic-assisted synthesis of doped TiO_2 nano-composites: Characterization and evaluation of photocatalytic and antimicrobial activity, Optik (Stuttg.) 127 (2016) 5171–5180. doi:10.1016/j.ijleo.2016.01.181

[43] R. Harichandran, N. Selvakumar, Effect of nano/micro B_4C particles on the mechanical properties of aluminium metal matrix composites fabricated by ultrasonic cavitation-assisted solidification process, Arch. Civ. Mech. Eng. 16 (2016) 147–158. doi:10.1016/j.acme.2015.07.001

[44] M. Bodunrin, K. Alaneme, L. Chown, Aluminium matrix hybrid composites: A review of reinforcement philosophies; mechanical, corrosion and tribological characteristics, J. Mater. Res. Technol. 4 (2015) 434–445. doi:10.1016/j.jmrt.2015.05.003

[45] M. Shamsipour, Z. Pahlevani, M. O. Shabani, A. Mazahery, Squeeze casting of electromagnetically stirred aluminum matrix nano-composites in semi-solid condition using hybrid algorithm optimized parameters, Kovove Mater. 55 (2017) 33–43. doi:10.4149/km_2017_1_33

[46] Y. Hao, Processing routes for aluminum based nanocomposites, Diss. Worcester Polytechnic Institute (2010).

[47] V. Shailesh, Evaporation and condensation of zinc, Masters Theses, (1971), 5106. https://scholarsmine.mst.edu/masters_theses/5106

[48] J. Hashim, L. Looney, M. Hashmi, Metal matrix composites: Production by the stir casting method, J. Mater. Process. Technol. 92 (1999) 1–7. doi:10.1016/S0924-0136(99)00118-1

[49] B. Bobić, S. Mitrović, M. Babić, A. Vencl, I. Bobić, Corrosion behavior of the as-cast and heat-treated ZA27 alloy, Tribol. Ind. 33 (2011) 87–93. doi:10.1016/S1003-6326(13)62550-9

[50] Z. Shao, Q. Le, Z. Zhang, J. Cui, Effect of ultrasonic power on grain refinement and purification processing of AZ80 alloy by ultrasonic treatment, Met. Mater. Int. 18 (2012) 209–215. doi:10.1007/s12540-012-2002-x

[51] B. Fatile, B. Adewuyi, H. Owoyemi, Synthesis and characterization of ZA-27 alloy matrix composites reinforced with zinc oxide nanoparticles, Eng. Sci. Technol. 20 (2017) 1147–1154. doi:10.1016/j.jestch.2017.01.001

[52] K. Ralston, D. Fabijanic, N. Birbilis, Effect of grain size on corrosion of high purity aluminium, Electrochim. Acta 56 (2011) 1729–1736. doi:10.1016/j.electacta.2010.09.023

[53] M. Spataru, M. Muntean, Electrical and mechanical properties of some high-alumina compositions obtained by the casting process of aqueous suspensions, Sci. Sintering 35 (2003) 37–40. doi:10.2298/SOS0301037S

[54] M. Almomani, M. Hayajneh, M. Draidi, Corrosion investigation of zinc-aluminum alloy matrix (ZA-27) reinforced with alumina (Al_2O_3) and fly ash, Part. Sci. Technol. 35 (2017) 439–447. doi:10.1080/02726351.2016.1165321

[55] L. Zheng, C. Fahe, L. Wenjuan, J. Bingli, J. Zhang, Corrosion behavior of pure zinc and its alloy under thin electrolyte layer, Acta Metall. Sin.-Engl. 23 (2010) 416–430. doi:10.11890/1006-7191-106-416

[56] G. Argade, S. Panigrahi, R. Mishra, Effects of grain size on the corrosion resistance of wrought magnesium alloys containing neodymium, Corros. Sci. 58 (2012) 145–151. doi:10.1016/j.corsci.2012.01.021